Supplement of Atmos. Chem. Phys., 25, 9831–9841, 2025
https://doi.org/10.5194/acp-25-9831-2025-supplement

Atmospheric Chemistry and Physics
Open Access
EGU

Supplement of

Fossil-dominated secondary organic aerosol (SOA) formation in coastal China: size-divergent pathways of aqueous Fenton reactions versus gas-phase volatile organic compound (VOC) autoxidation

Jia-Yuan Wang et al.

Correspondence to: Meng-Xue Tang (tangmx@pku.edu.cn)

Contents of this file

Text S1- Text S2

Text S1. More details of the source apportionment of WSOC by PMF modeling

Text S2. The experimental details for the 14C measurements

Figures S1- Figure S9

Figure S1. The map of the sampling site in southern China

Figure S2. The distribution of EV values for the three-factor solution based on PMF

Figure S3. The concentrations of species with standard deviations for the three-factor solution resolved in the PMF analysis

Figure S4. Comparison between the measured total mass of species and the PMF-reconstructed total mass of sources for WSOC(a), WSOO(b), CO_2^+(c), $C_4H_9^+$(d), and nss-K^+(e)

Figure S5. Diurnal variations of 10 selected VOCs during the campaign. Black lines and blue shading represent the mean and standard deviation, respectively

Figure S6. Particle size distribution of ALWC

Figure S7. Water-soluble transition metals in the fine and coarse mode

Figure S8. Particle size distribution of inorganic ions during different periods

Figure S9. Particle size distribution of $pH_{aerosol}$

Table S1 - Table S5

Table S1. Diagnostic parameters of BS and DISP error estimates of three factors of source analytic results of PMF model

Table S2. Molecular formula, uncertainty and limits of detection (LOD) of the measured VOCs species

Table S3. Summary of mass concentrations of gaseous pollutants (SO_2, NO_x, O_3), PM compositions (PM_1, $PM_{2.5}$, PM_{10}) and meteorological parameters (RH, Temperature (T), WS) during different periods according to this study.

Table S4. The correlation coefficients between OOC and typical inorganic ions in the campaign.

Table S5. The correlation coefficients between OOC and water-soluble metals in the campaign.

Text S1:More details of the source apportionment of WSOC by PMF modeling

The data matrices and error matrix of soluble organic carbon (WSOC), organic oxygen (WSOO), CO_2^+, $C_4H_9^+$, and nss-K^+ for a total of 160 samples (16 sets×10 stages) were input into the PMF model. The error matrix was processed according to the signal-to-noise ratio in the ToF-ACSM measurements. Nss-K^+ and CO_2^+ were included in the PMF modeling as tracers of primary biomass-burning organic aerosols (BBOA) and oxygenated organic aerosols (OOA), and $C_4H_9^+$ is a tracer of primary hydrocarbon-like organic aerosols (HOA) or exists in less oxidized organic aerosols as the oxidation product of HOA (Canagaratna et al., 2007; Cao et al., 2018; He et al., 2022; Huang et al., 2020). Two to five factors were tested for modeling, and the three-factor output (base run, Q_{true}/Q_{exp}=1.01) was found to be the most reasonable solution to explain all identified factor profiles, as will be discussed later; additionally, the solutions with more than three factors did not produce any new meaningful results for WSOC. The scaled residuals exhibited a generally symmetrical distribution between -3 and +3 as well. Moreover, there was also a strong overall correlation between the total factor concentrations reconstructed by the PMF model and the total mass concentrations of the measured species (Figure S4). All three factors were successfully mapped in 100% of the bootstrap (BS) runs, and no factor swaps were observed in the displacement (DISP) test. The absence of swaps indicates that the PMF results are sufficiently robust (Table S1). The derived EV values of the three-factor solution are shown in Figure S2, where the O/C ratio of each factor was calculated based on the WSOO/WSOC ratio for the factor. The nss-K^+ was allocated to factor 1, and the O/C ratio of this factor was 0.53; therefore, factor 1 was identified as biomass-burning organic carbon (BBOC). Factor 2 was identified as the more oxidized OOC (MO-OOC) due to its very high O/C ratio (1.85) and the predominant EV of CO_2^+.Almost all $C_4H_9^+$ were allocated to factor 3 and its moderate O/C (0.85); therefore, factor 3 was identified as the less oxidized oxygenated

organic carbon (LO-OOC), which is a reasonable result considering that LO-OOC can be partly formed by the oxidation of HOA (Cao et al., 2018). Therefore, it is reasonable to have the three-factor solution above as the most reasonable solution for size-resolved WSOC source apportionment at the study site.

Text S2: The experimental details for the ^{14}C measurements

Equal amounts of water extract of the same stages of MOUDI were combined and concentrated to less than 2 mL by a rotary evaporator and then a freeze drier, and finally titrated onto a quartz filter and placed in a desiccator to dry naturally. The dried filters were used to make graphite samples using the graphitization line at the Guangzhou Institute of Geochemistry, CAS through the hydrogen and zinc reduction method(Xu et al., 2007), and then graphite samples were measured with a compact accelerator mass spectrometry (NEC, National Electrostatics Corporation, USA) at the Guangzhou Institute of Geochemistry, CAS. AMS calibration was performed using standards (Oxalic Acid Standards I and II) and blanks. The $\delta^{13}C$ value was obtained during AMS measurements and applied to correct the ^{14}C measurements for isotopic fractionation. The fraction modern (f_{modern})was determined by comparing the measured $^{14}C/^{12}C$ ratio in a sample with that in a modern standard (NBS Oxalic Acid I in AD 1950). All of the reported f_{modern} values were corrected for $\delta^{13}C$ fractionation and for ^{14}C decay over the time period between 1950 and the year of measurement and more technical details can be found in the literatures (Zhang et al., 2019; Zhu et al., 2015).

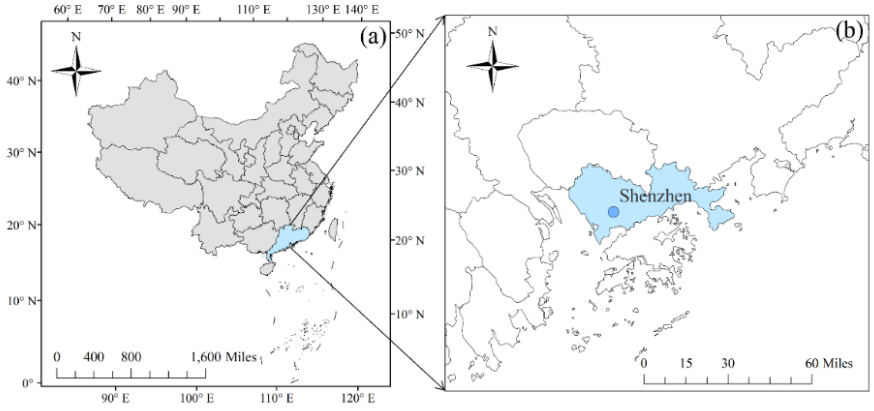

Figure S1. The map of the sampling site in southern China. The blue origin represents the sampling site.

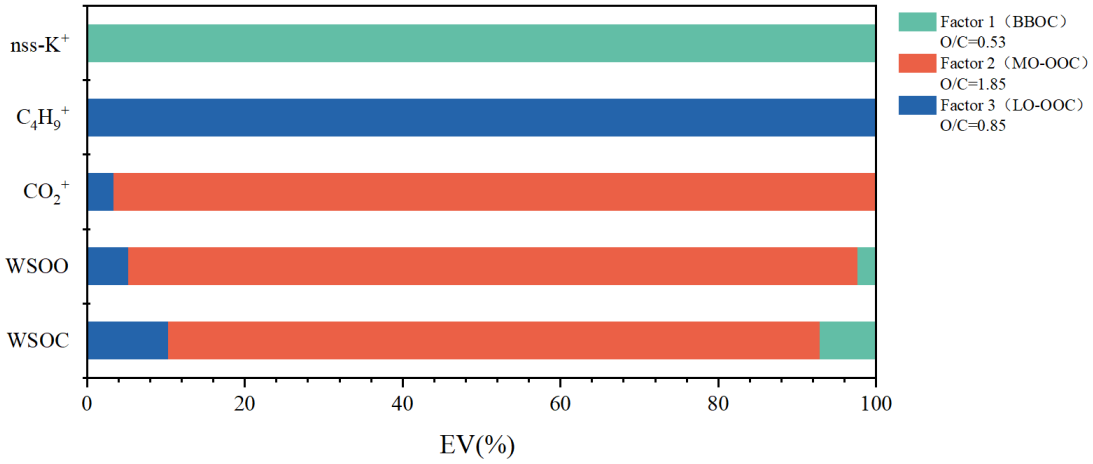

Figure S2. The distribution of EV values for the three-factor solution based on PMF.

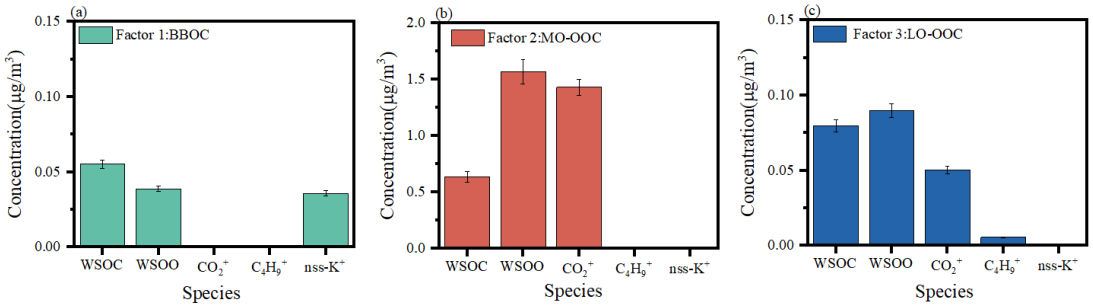

Figure S3. The concentrations of species with standard deviations for the three-factor solution resolved in the PMF analysis.

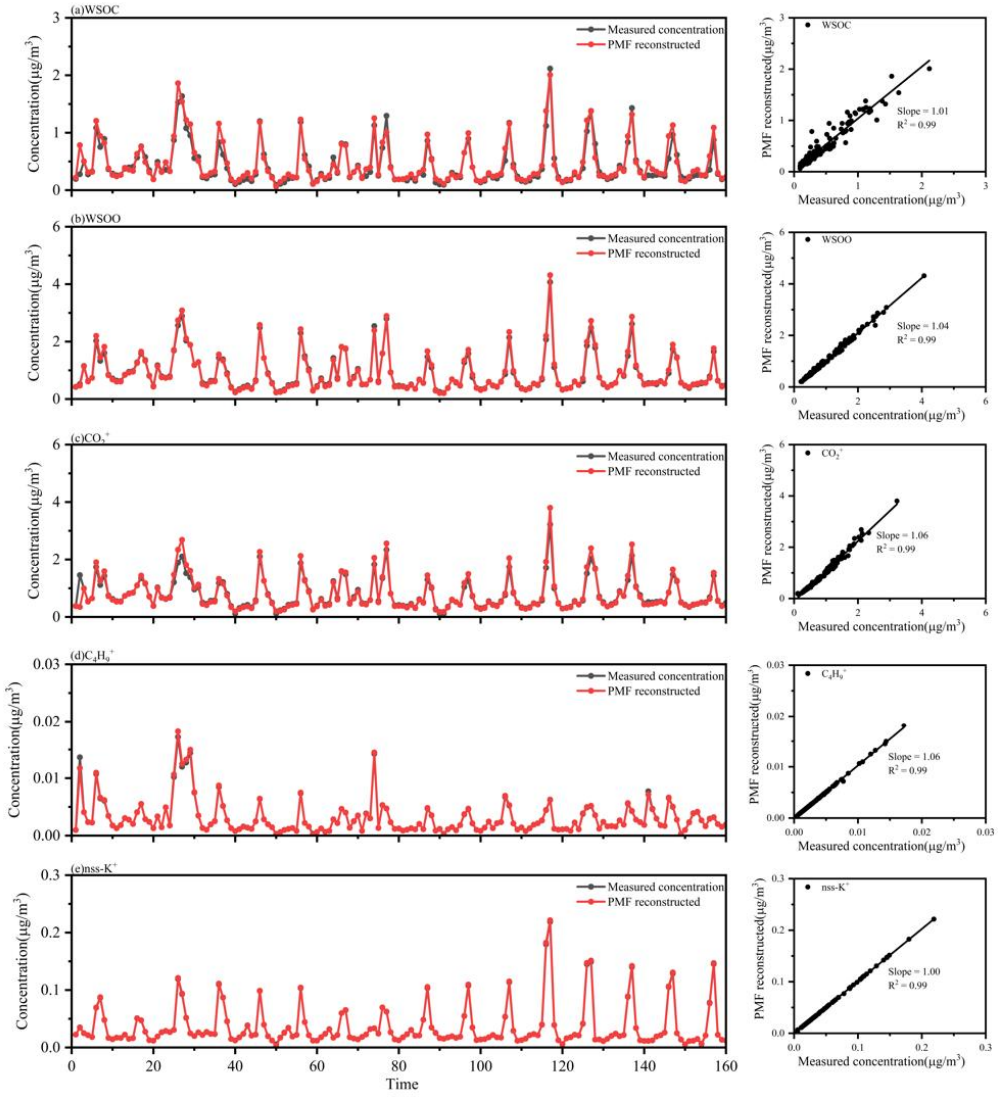

Figure S4. Comparison between the measured total mass of species and the PMF-reconstructed total mass of sources for WSOC(a), WSOO(b), CO_2^+(c), $C_4H_9^+$(d), and nss-K^+(e).

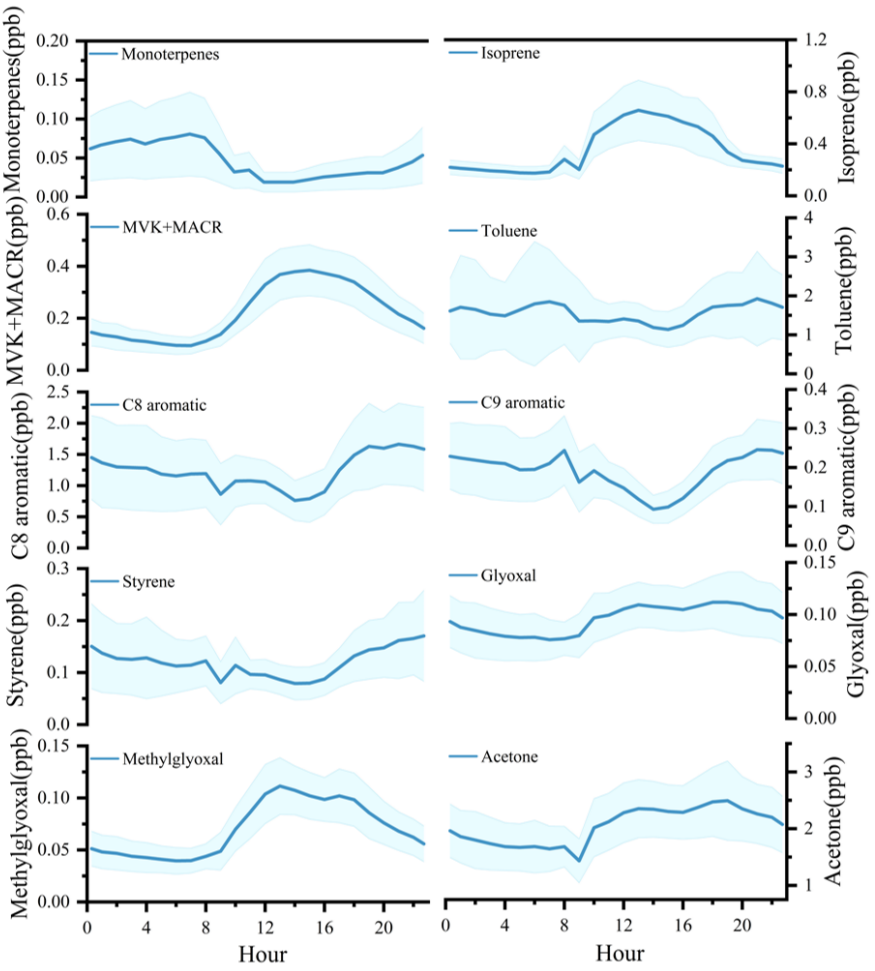

78

79 **Figure S5.** Diurnal variations of 10 selected VOCs during the campaign. Black lines and blue shading

80 represent the mean and standard deviation, respectively.

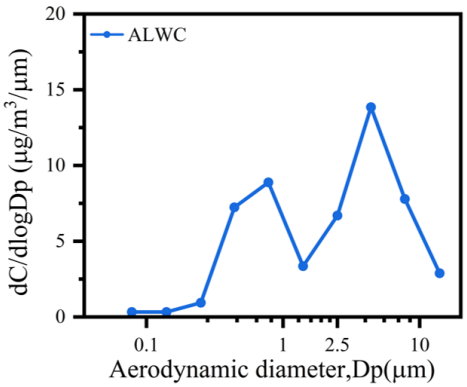

81

82 **Figure S6.** Particle size distribution of ALWC.

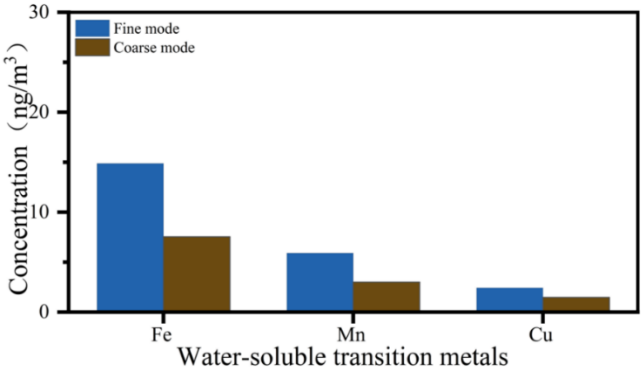

Figure S7. Water-soluble transition metals in the fine and coarse mode.

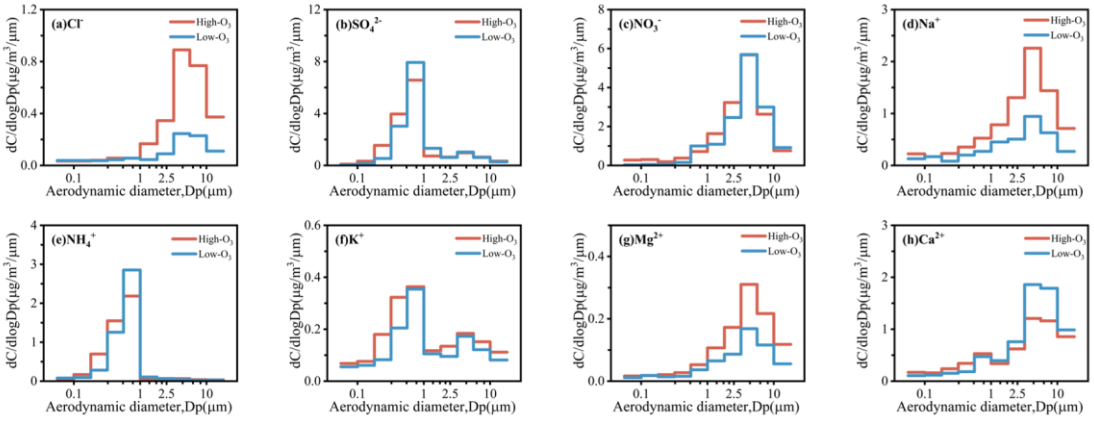

Figure S8. Particle size distribution of inorganic ions during different periods.

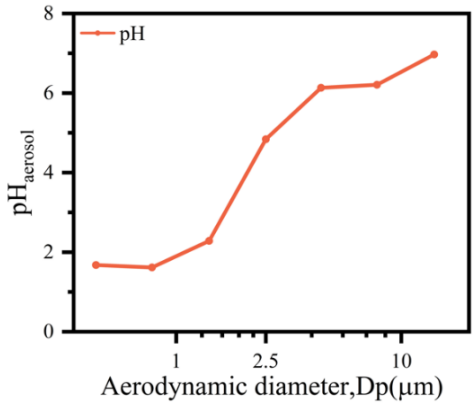

Figure S9. Particle size distribution of $pH_{aerosol}$.

Table S1. Diagnostic parameters of BS and DISP error estimates of three factors of source analytic results of PMF model.

diagnostics	Diagnostic parameters	3 factors
BS diagnostics	% BS mapping	100%
	% Unmapped	0
DISP diagnostics	Error Code	0
	Largest Decrease in Q	0
	%dQ	<0.1%
	Swaps by Factor	0

Table S2. Molecular formula, uncertainty and limits of detection (LOD) of the measured VOCs species.

Species	Molecular formula	m/z	Uncertainty	LOD
Monoterpenes	$C_{10}H_{16}$	136.23	9.7%	0.017
Isoprene	C_5H_8	68.06	5.5%	0.030
MVK+MACR	C_4H_6O	71.05	6.1%	0.034
Toluene	C_7H_8	92.06	3.2%	0.090
C8 aromatic	C_8H_{10}	107.13	4.8%	0.009
C9 aromatic	C_9H_{12}	121.15	6.9%	0.030
Styrene	C_8H_8	104.15	5.3%	0.021
Glyoxal	$C_2H_2O_2$	58.04	8.8%	0.017
Methylglyoxal	$C_3H_4O_2$	72.06	4.4%	0.039
Acetone	C_3H_6O	58.04	2.3%	0.150

Table S3. Summary of mass concentrations of gaseous pollutants (SO_2, NO_x, O_3), PM compositions (PM_1, $PM_{2.5}$, PM_{10}) and meteorological parameters (RH, Temperature (T), WS) during different periods according to this study.

Species	Entire study	High-O_3 period	Low-O_3 period
O_3 (μg/m^3)	68.26	96.52	67.13
NO_x (μg/m^3)	29.20	20.74	27.70
SO_2 (μg/m^3)	6.02	6.37	6.13
PM_1 (μg/m^3)	17.09	14.99	14.96
$PM_{2.5}$ (μg/m^3)	25.21	21.73	22.76
PM_{10} (μg/m^3)	44.10	43.78	41.35
RH (%)	61.27	58.25	72.83
T (°C)	20.0	24.4	24.2
WS (m/s)	0.9	1.2	0.6

Table S4. The correlation coefficients between OOC and typical inorganic ions in the campaign. * indicates a significance level of 95% ($p < 0.05$).

	SO_4^{2-}	NH_4^+	K^+	NO_3^-	Cl^-	Ca^{2+}
Fine mode OOC	0.85*	0.80*	0.81*	0.47	0.53	0.34
Coarse mode OOC	0.15	0.26	0.27	0.10	0.16	-0.30

Table S5. The correlation coefficients between OOC and water-soluble metals in the campaign. * indicates a significance level of 95% ($p < 0.05$).

	Cu	Fe	Mn
Fine mode OOC	0.31	0.82*	0.55
Coarse mode OOC	0.64	0.57	0.40

References

Boreddy, S. K. R. and Kawamura, K.: A 12-year observation of water-soluble ions in TSP aerosols collected at a remote marine location in the western North Pacific: an outflow region of Asian dust, Atmospheric Chem. Phys., 15, 6437–6453, 2015.

Canagaratna, M. R., Jayne, J. T., Jimenez, J. L., Allan, J. D., Alfarra, M. R., Zhang, Q., Onasch, T. B., Drewnick, F., Coe, H., Middlebrook, A., Delia, A., Williams, L. R., Trimborn, A. M., Northway, M. J., DeCarlo, P. F., Kolb, C. E., Davidovits, P., and Worsnop, D. R.: Chemical and microphysical characterization of ambient aerosols with the aerodyne aerosol mass spectrometer, Mass Spectrom. Rev., 26, 185–222, 2007.

Cao, L.-M., Huang, X.-F., Li, Y.-Y., Hu, M., and He, L.-Y.: Volatility measurement of atmospheric submicron aerosols in an urban atmosphere in southern China, Atmospheric Chem. Phys., 18, 1729–1743, 2018.

Dai, Q., Schulze, B. C., Bi, X., Bui, A. A. T., Guo, F., Wallace, H. W., Sanchez, N. P., Flynn, J. H., Lefer, B. L., Feng, Y., and Griffin, R. J.: Seasonal differences in formation processes of oxidized organic aerosol near Houston, TX, Atmospheric Chem. Phys., 19, 9641–9661, 2019.

Duan, J., Huang, R.-J., Li, Y., Chen, Q., Zheng, Y., Chen, Y., Lin, C., Ni, H., Wang, M., Ovadnevaite, J., Ceburnis, D., Chen, C., Worsnop, D. R., Hoffmann, T., O'Dowd, C., and Cao, J.: Summertime and wintertime atmospheric processes of secondary aerosol in Beijing, Atmospheric Chem. Phys., 20, 3793–3807, 2020.

Feng, T., Wang, Y., Hu, W., Zhu, M., Song, W., Chen, W., Sang, Y., Fang, Z., Deng, W., Fang, H., Yu, X., Wu, C., Yuan, B., Huang, S., Shao, M., Huang, X., He, L., Lee, Y. R., Huey, L. G., Canonaco, F., Prevot, A. S. H., and Wang, X.: Impact of aging on the sources, volatility, and viscosity of organic aerosols in Chinese outflows, Atmospheric Chem. Phys., 23, 611–636, 2023.

He, D.-Y., Huang, X.-F., Wei, J., Wei, F.-H., Zhu, B., Cao, L.-M., and He, L.-Y.: Soil dust as a potential bridge from biogenic volatile organic compounds to secondary organic aerosol in a rural environment, Environ. Pollut., 298, 118840, https://doi.org/10.1016/j.envpol.2022.118840, 2022.

Hu, W., Hu, M., Hu, W.-W., Zheng, J., Chen, C., Wu, Y., and Guo, S.: Seasonal variations in high time-resolved chemical compositions, sources, and evolution of atmospheric submicron aerosols in the megacity Beijing, Atmospheric Chem. Phys., 17, 9979–10000, 2017.

Huang, X.-F., Dai, J., Zhu, Q., Yu, K., and Du, K.: Abundant Biogenic Oxygenated Organic Aerosol in

Atmospheric Coarse Particles: Plausible Sources and Atmospheric Implications, Environ. Sci. Technol., 54, 1425–1430, 2020.

Klopper, D., Formenti, P., Namwoonde, A., Cazaunau, M., Chevaillier, S., Feron, A., Gaimoz, C., Hease, P., Lahmidi, F., Mirande-Bret, C., Triquet, S., Zeng, Z., and Piketh, S. J.: Chemical composition and source apportionment of atmospheric aerosols on the Namibian coast, Atmos Chem Phys, 2020.

Sun, Y., Du, W., Fu, P., Wang, Q., Li, J., Ge, X., Zhang, Q., Zhu, C., Ren, L., Xu, W., Zhao, J., Han, T., Worsnop, D. R., and Wang, Z.: Primary and secondary aerosols in Beijing in winter: sources, variations andprocesses, Atmospheric Chem. Phys., 16, 8309–8329, 2016.

Sun, Y., Xu, W., Zhang, Q., Jiang, Q., Canonaco, F., Prévôt, A. S. H., Fu, P., Li, J., Jayne, J., Worsnop, D. R., and Wang, Z.: Source apportionment of organic aerosol from 2-year highly time-resolved measurements by an aerosol chemical speciation monitor in Beijing, China, Atmospheric Chem. Phys., 18, 8469–8489, 2018.

Wei, F., Peng, X., Cao, L., Tang, M., Feng, N., Huang, X., and He, L.: Characterizing water solubility of fresh and aged secondary organic aerosol in PM2.5 with the stable carbon isotope technique, Atmospheric Chem. Phys., 24, 8507–8518, 2024.

Xu, W., Xie, C., Karnezi, E., Zhang, Q., Wang, J., Pandis, S. N., Ge, X., Zhang, J., An, J., Wang, Q., Zhao, J., Du, W., Qiu, Y., Zhou, W., He, Y., Li, Y., Li, J., Fu, P., Wang, Z., Worsnop, D. R., and Sun, Y.: Summertime aerosol volatility measurements in Beijing, China, Atmospheric Chem. Phys., 19, 10205–10216, 2019.

Xu, X., Trumbore, S. E., Zheng, S., Southon, J. R., McDuffee, K. E., Luttgen, M., and Liu, J. C.: Modifying a sealed tube zinc reduction method for preparation of AMS graphite targets: Reducing background and attaining high precision, Nucl. Instrum. Methods Phys. Res. Sect. B Beam Interact. Mater. At., 259, 320–329, 2007.

Zhang, X., Li, J., Mo, Y., Shen, C., Ding, P., Wang, N., Zhu, S., Cheng, Z., He, J., Tian, Y., Gao, S., Zhou, Q., Tian, C., Chen, Y., and Zhang, G.: Isolation and radiocarbon analysis of elemental carbon in atmospheric aerosols using hydropyrolysis, Atmos. Environ., 198, 381–386, 2019.

Zhu, S., Ding, P., Wang, N., Shen, C., Jia, G., and Zhang, G.: The compact AMS facility at Guangzhou Institute of Geochemistry, Chinese Academy of Sciences, Nucl. Instrum. Methods Phys. Res. Sect. B Beam Interact. Mater. At., 361, 72–75, 2015.